RSC Advances

PAPER

View Article Online
View Journal | View Issue

Cite this: *RSC Adv.*, 2022, **12**, 30045

Benzothiazole appended 2,2′-(1,4-phenylene) diacetonitrile for the colorimetric and fluorescence detection of cyanide ions†

Dhanapal Jothi, [a] Sathishkumar Munusamy,[b] Saravanakumar Manickam,[c] Saravanan Enbanathan, [a] Selin Manojkumar[a] and Sathiyanarayanan Kulathu Iyer *[a]

A benzothiazole appended 2,2′-(1,4-phenylene)diacetonitrile derivative (2*Z*,2′*Z*)-2,2′-(1,4-phenylene)bis(3-(3-(benzo[*d*]thiazol-2-yl)-4-hydroxyphenyl)acrylonitrile) (**PDBT**) has been synthesized and investigated as a novel sensor, capable of showing high selectivity and sensitivity towards CN^- over a wide range of other interfering anions. After reaction with CN^-, **PDBT** shows a new absorption peak at 451 nm with a color transformation from colorless to reddish-brown. When yellow fluorescent PDBT is exposed to CN^-, it displays a significant increase in fluorescence at 445 nm, resulting in strong sky-blue fluorescence emission. The nucleophilic addition reaction of CN^- plays a role in the sensing mechanism of **PDBT** to CN^-. **PDBT** can distinguish between a broad variety of interfering anions and CN^- with remarkable selectivity and sensitivity. Furthermore, the detection limit of the **PDBT** probe for CN^- is 0.62 μM, which is significantly lower than the WHO standard of 1.9 μM for drinking water. Density functional theory simulations corroborated the observed fluorescence changes and the internal charge transfer process that occurs after cyanide ion addition. In addition, real-time applications of **PDBT**, such as cell imaging investigations and the detection of CN^- in water samples, were successfully carried out.

Received 15th June 2022
Accepted 27th September 2022

DOI: 10.1039/d2ra03702e

rsc.li/rsc-advances

Introduction

Since they are so prevalent, anionic species serve a critical role in a broad range of biological and chemical processes.[1–6] Their inappropriate release pollutes the environment, endangering all life forms as a direct consequence.[7–9] A well-known and contentious anion among the numerous anions is cyanide (CN^-), which has piqued researchers' curiosity for a long time. Cyanide has applications in numerous chemical processes, including extraction of precious metals, electroplating, metallurgy, tanning, medicine and plastic manufacturing, *etc.*[10–14] Additionally, chemical warfare agents and pesticides both employ cyanide gas as a method of extermination. Inadequate control over the usage of CN^- in the environment might lead to the substance entering the body. At relatively low concentrations, CN^- binds to cytochrome's ferric ions in the mitochondrial respiratory chain, inhibiting oxygen carriage and causing cell death.[15,16] Water cyanide levels are limited by the World Health Organization (WHO) to 70 μM for long-term exposure and 500 μM for short-term exposure. Unfortunately, the likelihood of cyanide exposure has increased in recent years due to both accidental and intentional exposure. Thus, environmental cyanide detection has received crucial attention, pushing us to create a low-cost and robust sensor that can detect CN^- in real water samples and living cells.

Colorimetric and fluorescence sensors have garnered a great deal of interest because of their practicality, high sensitivity, and selectivity, as well as their ability to be detected with the "naked eye" and potential use in bioimaging.[17–25] Colorimetric and fluorimetric sensors have been used in multiple studies to date to detect cyanide anion utilizing different sensing methods, such as supramolecular self-assembly, nucleophilic addition, and hydrogen bonds. Some of the most important electron-deficient sites in nucleophilic addition-based sensing probes were benzothiazole, malononitrile, and dialkyl malate.[26–36] Notwithstanding, most sensors have a complicated synthesis process, a poor color response, and a low level of sensitivity. Furthermore, methods for cyanide detection employing hydrogen bonding interaction have limitations when used in conjunction with anions that are competitive, such as fluoride, acetate, and phosphate ions.

[a]*Department of Chemistry, School of Advanced Sciences and Vellore Institute of Technology, Vellore-632014, India. E-mail: sathiya_kuna@hotmail.com*
[b]*Institute of Chemical Biology and Nanomedicine, State Key Laboratory of Chemo/Biosensing and Chemometrics, College of Chemistry and Chemical Engineering, Hunan University, Changsha 410082, P.R. China. E-mail: pra3sat@gmail.com*
[c]*Saveetha School of Engineering, Saveetha Institute of Medical and Technological Sciences, (SIMATS), Chennai-602105, Tamil Nadu, India. E-mail: solorsaravanan50@gmail.com*

† Electronic supplementary information (ESI) available. See https://doi.org/10.1039/d2ra03702e

This observation led us to introduce a benzothiazole unit in 2,2′-(1,4-phenylene)diacetonitrile through a conjugated double bond, which is predicted to display strong electrophilic character and lead to the nucleophilic addition of cyanide. The synthesized receptor **PDBT** has expanded π-conjugation between two benzothiazole units along strong electron acceptor phenylenediacetonitrile. Therefore, the cyanide ion attack on the **PDBT** was predicted to disrupt the conjugation mechanism as well as the ICT procedure.[37–43] A modification in intramolecular conformation in the subsequent cyanide product significantly alters receptor **PDBT** absorption and emission characteristics. The chemosensor **PDBT** shows a bright brown color over the addition of micromolar quantities of CN^-, enabling it to be utilized for effective naked eye detection of CN^- ion.

Experimental section

All the required chemical reagents were purchased from Alfa Aesar and sigma Aldrich, and they were utilized directly without further purification. Especially, Solvents (analytical grade) were purchased from Pure chem. NMR (Nuclear Magnetic Resonance) spectra were recorded on Bruker Ascent-400 spectrometer. Chemical shifts (δ) are represented in the measure of ppm and TMS has been fixed as an internal standard. To identify the exact mass of the compound, High-Resolution Mass Spectral (HRMS) measurements were carried out in Waters – Xevo G2 – XS – Q ToF High Resolution Mass spectrometer instrument. Furthermore, fluorescence emission and absorption spectrum were recorded by PerkinElmer LS-55 luminescence spectrometer and Shimadzu 3600 spectrophotometer respectively. To evaluate the biological interaction of **PDBT** with CN^- ions in the living cells, fluorescent live cell images were recorded in WEWOX fluorescence microscope 3000.

Synthesis of 3-(benzo[*d*]thiazol-2-yl)-4-hydroxybenzaldehyde (SMD)

The compound **SMD** was prepared by the formylation of 2-(benzo[*d*]thiazol-2-yl)phenol with hexamethylenetetramine (HMTA) in acetic acid under reflux condition for 5 hours. The further procedures were followed as per the literature.[44,46]

Synthesis of PDBT

1,4-Phenylenediacetonitrile (312.0 mg, 2.0 mmol) was dissolved in dry DMF (10 mL) and potassium *tert*-butoxide (220.0 mg, 2.0 mmol) was added. The resulting solution was stirred under nitrogen atmosphere at 90 °C for 20 minutes. To this reaction mixture, **SMD** was added (1.02 g, 4.0 mmol) and the reaction mixture was allowed to stir under N_2 atmosphere at 90 °C for a further period of 3 h. The appearance of new orange fluorescence spot in TLC confirms the formation of compound (**PDBT**). After confirming the completion of the reaction by TLC, the reaction mixture was allowed to cool to room temperature, diluted with H_2O, neutralized by adding hydrochloric acid, and extracted with ethyl acetate three times. The extracted organic layers were dried by adding anhydrous Na_2SO_4. Ethyl acetate was removed under reduced pressure, and the concentrated residue was purified by silica gel column chromatography. Yield 73% (280 mg). ^{1}H NMR (400 MHz, DMSO-d_6)™: δ 7.204–7.220 (d, 2H, J = 2.87), 7.382–7.406 (m, 7H, J = 2.95 Hz), 7.807–7.824 (d, 4H, J = 3.12 Hz), 8.126–8.145 (m, 8H, J = 3.24 Hz), 13.048 (s, 1H). ^{13}C NMR (DMSO-d_6, 100 MHz): δ 108.54, 119.65, 120.88, 121.06, 121.77, 122.77, 122.98, 125.40, 125.49, 125.72, 128.56, 129.28, 129.31, 129.75, 129.89, 131.39, 135.87, 136.10, 142.03, 152.24, 166.17.

Results and discussion

The cyanide chemosensor **PDBT** was synthesized from commercially accessible materials in a single step using the Knoevenagel condensation method. As shown in Scheme 1, **PDBT** was synthesized in 73% yield from 3-(benzo[*d*]thiazol-2-yl)-4-hydroxybenzaldehyde and 2,2′-(1,4-phenylene)diacetonitrile. Having synthesized the receptor **PDBT**, it was characterized by NMR and mass spectroscopy analysis (Fig. S1–S3†).

UV-vis and emission spectral responses of PDBT towards CN^- ion

To test its sensitivity to different anions, the **PDBT** probe (10 μM) in CH_3CN : H_2O (1 : 1, v/v) solution was exposed to a variety of anions, including F^-, Cl^-, Br^-, I^-, OAc^-, CN^-, ClO_4^-, $H_2PO_4^-$, HCO_3^-, HSO_4^-, SH^-, NO_3^-, SCN^-, S^{2-}, and OH^- and examined by the naked eye and UV-vis spectral studies. Individual electronic spectra of **PDBT** with various selective anions are shown in Fig. S8.† The probe (**PDBT**) was evaluated for selectivity with ten equivalents of different anions and only CN^- showed a significant color shift from colorless to reddish-brown in the experiments (Fig. 1a). Also, UV-vis spectroscopy was used to examine spectral shifts of **PDBT** over the addition CN^-, which confirmed that the probe was selective for the CN^- ion. **PDBT** alone has two absorption bands in the spectra, with the higher intensity peak at 298 nm and the peak at 365 nm has low intensity (Fig. 1b). The π–π* and n–π* transitions are considered to be responsible for the formation of these bands. Adding CN^- reduced the absorption at 365 nm and created a new absorption at 451 nm. However, the absorption at 298 nm was largely unaffected.

A distinct isosbestic point at 400 nm was generated due to the absorption alterations in **PDBT** caused by the addition of CN^- (Fig. 1c). An absorbance titration in CH_3CN : H_2O (v/v, 1 : 1) was carried out to learn more about the interaction between **PDBT** and CN^-. The UV absorbance band centred at 365 nm reduced progressively when CN^- ions were added to the probe **PDBT** solution, while a new, virtually wide peak gradually developed at 451 nm. It was possible to acquire an accurate

Scheme 1 Synthesis of probe PDBT.

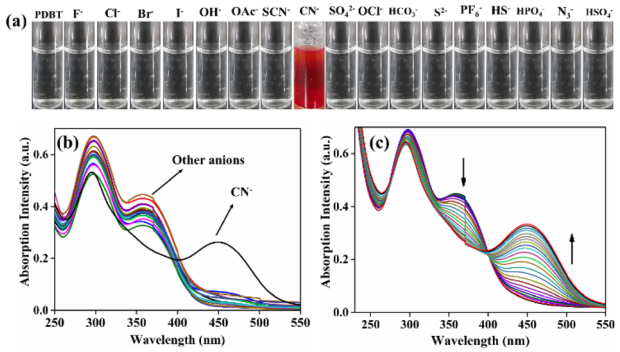

Fig. 1 (a) Probe **PDBT** (CH_3CN : H_2O, 1 : 1 v/v) naked-eye test with the addition of 10 equivalents of different anionic salt solutions (b) change in the UV-vis spectra of **PDBT** (10 μM) in the presence of various anions (c) sensitivity of **PDBT** (10 μM) with increasing concentration of cyanide ion from 1×10^{-5} M to 2×10^{-5} M.

linear range of 1–20 μM using UV-vis absorption titration data and a correlation coefficient $R^2 = 0.9933$ (Fig. S4†).

The aqueous solutions containing 5 μM of different relevant competitive analytes (as assessed in the UV-vis study) were used to investigate the **PDBT**'s selectivity and competitivity for the identification of CN^-. When the aforementioned competing species were individually added to a 1 μM **PDBT** solution, the probe solution showed minor fluorescence intensity change at 576 to 445 nm towards those relevant analytes, as shown in Fig. 2a. When only 2 μM CN^- was added to the probe solution, nevertheless, the intensity of the fluorescence spectrum of **PDBT** was dramatically improved. The findings confirmed that **PDBT** has a high selectivity for cyanide ions. Meanwhile, the fluorescence spectra of **PDBT** with and without CN^- ion has a marked difference. **PDBT** alone has a strong emission peak at 576 nm, showing orange fluorescence. In the presence of CN^-, the fluorescence emission at 576 nm begins to decline, and a new emission peak at 445 nm starts to rise. Consequently, the **PDBT** solution's initial orange fluorescence begins to fade and is progressively replaced by an intense greenish-blue fluorescence (Fig. 2b). The observed change in the fluorescence emission of **PDBT** in the presence of CN^- indicated the potential of quantifying CN^- detection using a ratiometric response. The change in the F_{576}/F_{445} ratio with increasing CN^- concentration is shown graphically in Fig. 2c. When the concentration of CN^- was raised from 0 to 2 μM, the fluorescence ratio F_{576}/F_{445} was enhanced by approximately six-fold. It is also important to note that the F_{576}/F_{445} ratio responds linearly to CN^- concentrations in the range of 0.1–1 μM. A fluorescence spectrum titration was used to compute LOD (limit of detection) using the formula $LOD = 3\sigma/K$, where σ is the standard deviation of blank measurements (Fig. S9†) and K is the slope of the plot of fluorescence intensity ratio (F_{576}/F_{445}) *versus* sample concentration. As a result, a LOD of 0.62 μM was determined.

The ability to resist interference from competing analytes is a critical measure of the reliability of fluorescence sensor identification. As shown in Fig. 2d, the probe **PDBT** was inert to the addition of the other pertinent anions; however, the emission intensity of **PDBT** at 576 and 445 nm has experienced a radical transformation following the addition of CN^-. These findings demonstrated that the detection of the cyanide anion by the probe **PDBT** was not affected by the presence of other competing anions. Overall, the findings indicated that **PDBT** had greater selectivity and anti-interference to CN^- than other relevant analytes in this study.

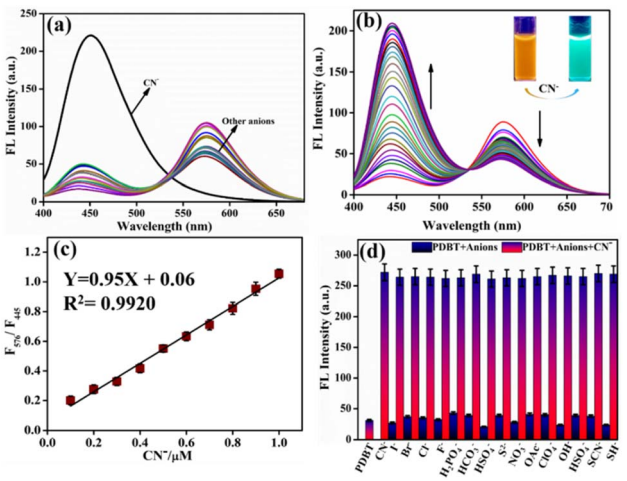

Fig. 2 (a) Emission selectivity spectra of **PDBT** (1 μM) in the presence of various anions. (b) Emission spectra of **PDBT** (1 μM) in the presence of various concentrations of CN^- (0–2 μM) in CH_3CN : H_2O (v/v, 1 : 1). Inset: photographic images of the **PDBT** solution before and after CN^- was added. (c) Fluorescence ratios of **PDBT** (F_{576}/F_{445}) against CN^- concentrations. $\lambda_{ex} = 365$ nm. Slits width: 5/5 nm. Error bars are ± SD, $n = 3$. (d) Interference of **PDBT** in acetonitrile/water (1 : 1, v/v) medium in the presence of CN^- and other anions.

Effect of pH and time

To determine the effect of pH on the detection of probe PDBT, the response of PDBT (1 μM) was evaluated in a 1 : 1 mixture of CH_3CN and H_2O to CN^- (2 μM) when the pH is between 2 and 12. As depicted in Fig. 3a, the intensity of **PDBT** without cyanide ion at 576 nm was stable at a low level within a wide pH range of 2–12. For the pH range 2 to 12, **PDBT**'s fluorescence signal at 445 nm was found to be very weak and only minimally affected by H^+ or OH^-. When 2 μM CN^- was added to a **PDBT** solution, the emission intensity at 445 nm rise significantly. It has been shown

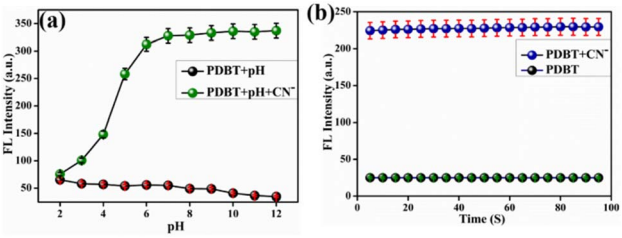

Fig. 3 (a) Stability of sensor compound **PDBT** at 445 nm in the presence and absence of CN^-(2 μM) in different pH conditions in acetonitrile/water (1 : 1, v/v) solvent system. (b) Chemical kinetics studies of probe **PDBT** upon the addition of CN^-.

that when CN^- is present at pH values between 2 and 12, the fluorescence intensity at 445 nm of the sensor PDBT rises significantly. It has also been demonstrated that the fluorescence response to CN^- between 6 and 12 was practically pH-independent. In a 1 : 1 combination of CH_3CN and H_2O, the temporal relevance of **PDBT** (1 μM) on CN^- (2 μM) is illustrated in Fig. 3b. In the existence of CN^-, the emission intensity at 445 nm immediately increased and reached a stable value within 5 seconds of playing time, which implied that fluorescence recording of **PDBT** can be taken immediately over the addition of CN^-. When CN^- was present, the emission intensity at 445 nm surged instantly and reached a steady value after 5 seconds of recording time, indicating that fluorescence recording of **PDBT** could be performed immediately after the addition of CN^-.

Investigation of sensing mechanism

The chemosensor and analyte stoichiometric ratio are critical in determining the sensing mechanism. Job's plot was used to investigate the binding stoichiometry of the chemosensor **PDBT** with CN^- to establish the mechanism. Job's figure was created by plotting the fluorescence intensity ratio (F_{576}/F_{445}) as a function of the **PDBT**/(**PDBT** + CN^-). According to Job's figure, the highest emission intensity of **PDBT** chemosensors was seen at 0.4 mol fraction of CN^- ions (binding stoichiometry; 1 : 2). (Fig. S5†). This 1 : 2 binding stoichiometry demonstrates that two molecules of CN^- react with one molecule of **PDBT**. In addition, the HRMS results of dye **PDBT** at 629.0978 and probe **PDBT** + CN^- ions show a new peak at $m/z = 685.12$, supporting this finding (Fig. S6†).

Furthermore, the detection mechanism of the chemosensor in the presence of CN^- was investigated using a ^{1}H NMR titration experiment in DMSO-d_6 (Fig. 4). Fig. 4a shows that probe **PDBT** displays a characteristic peak corresponding to phenolic (–OH) proton at 12.92 ppm. The vinyl proton signals at 8.21 ppm fade after the titration with CN^- to the probe, and a new signal resonates at 7.30 ppm. The aromatic proton Ha, as represented in Fig. 4, shifts to the upfield region from 7.18 ppm to 6.48 ppm. Furthermore, the aromatic proton signals have been displaced to a certain degree. The presence of a new peak at 7.30 ppm has been linked to cyano ethyl proton. It proves that CN^- ions attack the vinyl group *via* nucleophilic addition reaction.

In addition, density functional theory (DFT) calculations were done using the Gaussian 09 software to ascertain the sensing mechanism's viability. The B3LYP/6-31G (d) level of theory was used to optimize the geometries and frontier molecular orbital (FMO) analyses of both chemosensors and the targeted product. Fig. S7† and 5 reveal the HOMO–LUMO surfaces of chemosensor **PDBT**. The transition energies and relative oscillator strengths of the probable important transitions for the **PDBT** and **PDBT** + CN^-, have been found (Table S1†). The HOMO orbital was restricted to the central core of **PDBT**, which has the phenyl ring connected by two cyano units, whereas the LUMO orbital was diffused around the dicyanophenyl unit of **PDBT**, but with a higher electron density. However, in the **PDBT** + CN^- complex, the electron density of the HOMO orbital is more distributed on the benzothiazole unit than on the dicyanophenyl unit. In LUMO orbitals, on the other hand, electrons are localized on the dicyanophenyl unit. This behaviour is attributable to the breakdown of extended conjugation of the chemosensor after the interaction of CN^- with the vinyl group of **PDBT**. Additionally, the rupture of the π-conjugated structure leads to a significant HOMO–LUMO energy difference (3.49 eV) for sensor **PDBT** + CN^- than for sensor **PDBT** (3.27 eV). As a result of these theoretical calculations, it was determined that CN^- attacked the C=C link and disrupted the molecule's conjugation structure, resulting in decreased ICT in sensor **PDBT** + CN^-.

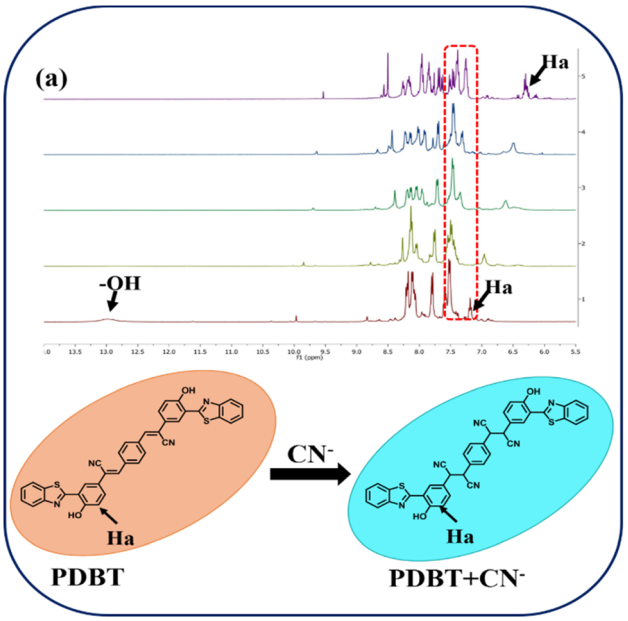

Fig. 4 (a) ^{1}H NMR titration of PDBT with the incremental addition of 1 equiv. of CN^- ions in DMSO-d_6 solvent.

Application in natural water samples

To determine the chemosensor **PDBT**'s suitability for practical use, spiked CN^- levels in tap water samples were monitored

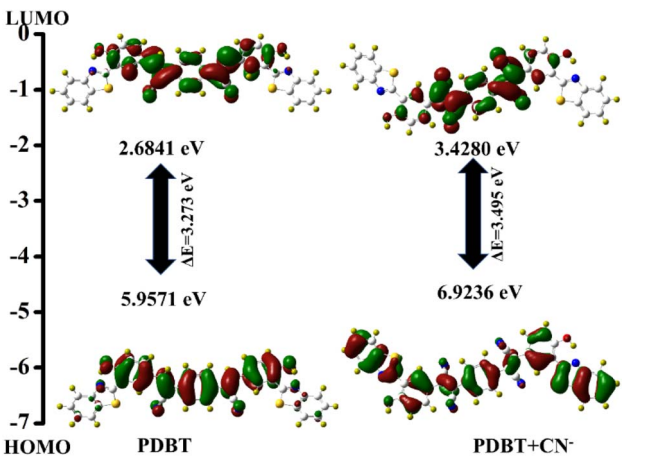

Fig. 5 Frontier molecular orbital diagram for PDBT and PDBT + CN^-.

Table 1 The determination of spiked CN^- in tap water

Spiked (μM)	Detected (μM)	Average (μM)	Recovery (%)	RSD (%)
1	0.95	0.96	95	1.04
	0.97		97	
	0.96		96	
2	1.93	2.0	96	3.40
	2.02		101	
	2.05		102.5	
3	2.92	2.90	97	0.6
	2.89		96	
	2.90		96	

(from the campus of Vellore Institute of Technology). As established by the fluorescence standard curve and the cyanide concentration, tap water was tested three times for the presence of cyanide (CN^-).

As indicated in Table 1, the chemosensor **PDBT** displayed great consistency in detecting CN^- in water samples. The relative standard deviations (RSD.) and recoveries were computed using the relevant figures. The findings of the experiments demonstrated that the optical probe **PDBT** exhibited good accuracy in detecting quantitative cyanide in aqueous solutions. An exciting practical use for this technology is in monitoring cyanide in gold leach waste solutions that include cyanide and other solutions that have larger concentrations of cyanide ions.

Cell imaging

Probe **PDBT** was used to detect CN^- in *Escherichia coli* cells to test the bioimaging capabilities of the probe.[45] According to the bright field diagram (Fig. 6a), it is clear that healthy cell morphology was seen in the experiment, showing that the probe was biocompatible and cytotoxicity-free. When fluorescence microscopy was used to examine the cell area, it revealed a significant bright yellow fluorescence inside the cells, and the probe has good cell membrane permeability. Furthermore, the cells showed a blue-green fluorescence after being treated with probe **PDBT** (2 μM) and subsequently treated with CN^- (5 μM). Based on these findings, it is obvious that the probe **PDBT** may be employed to detect the presence of exogenous CN^- in live cells.

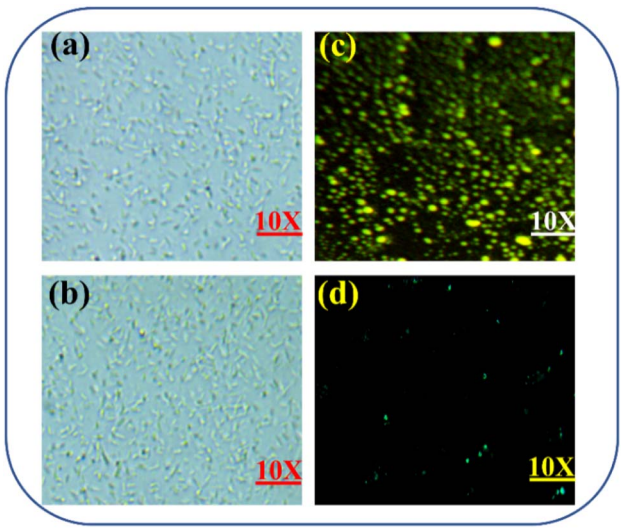

Fig. 6 Fluorescence microscopic photographs of *Escherichia coli* cells incubated with PDBT (2 μmol L^{-1}) for CN^- ion detection. PDBT was excited at 365 nm, and fluorescence was collected at 430–550 nm. Scale bar: 10 μm. (a) and (b) Bright field images of *E. coli* cells; (c) fluorescent field image of PDBT treated *E. coli* cells; (d) fluorescent field image of PDBT treated *E. coli* cells incubated with CN^- ions.

Conclusion

In conclusion, by coupling 3-(benzo[*d*]thiazol-2-yl)-4-hydroxybenzaldehyde on either side of 2,2′-(1,4-phenylene) diacetonitrile, an efficient and straightforward colorimetric and ratiometric chemosensor **PDBT** has been effectively achieved. The interaction of **PDBT** with anions was investigated using UV-vis and fluorescence techniques. The chemosensor **PDBT** demonstrated great sensitivity and a sole reaction to CN^- with a LOD of 0.62 μM. Spectral experiments and theoretical calculations have shown that the nucleophilic addition of CN^- to the sensor **PDBT** causes an interruption in the conjugated structure of the molecule, resulting in the inhibition of ICT and, therefore, the optical changes. Finally, **PDBT** was successfully proven in real-time samples for practical applications and live-cell imaging, indicating that **PDBT** may function as a qualitative and a quantitative sensor for the detection of CN^- ions.

Conflicts of interest

There are no conflicts to declare.

Acknowledgements

Dhanapal J. sincerely thanks Vellore Institute of Technology for providing a Teaching Cum Research Assistant (Project No: VIT/HR/2019/12732) for the financial support. The DST-FIST NMR facility at VIT University is duly acknowledged. The authors thank Dr S. Meenakshi, SSL-VIT for language editing.

References

1 L. K. Macreadie, A. M. Gilchrist, D. A. McNaughton, W. G. Ryder, M. Fares and P. A. Gale, *Chem*, 2022, **8**, 46–118.
2 J. Yang, W. Tai, F. Wu, K. Shi, T. Jia, Y. Su, T. Liu, P. Mocilac, X. Hou and X. Chen, *Chemosphere*, 2022, **292**, 133401.
3 X. Huang, L. Huang, S. R. B. Arulmani, J. Yan, Q. Li, J. Tang, K. Wan, H. Zhang, T. Xiao and M. Shao, *Environ. Res.*, 2022, **204**, 112381.
4 N. Chen and Y. M. Lee, *Trends Chem.*, 2022, DOI: 10.1016/j.trechm.2021.12.009.
5 Á. J. Patiño-Agudelo and F. H. Quina, *J. Colloid Interface Sci.*, 2022, **611**, 39–45.
6 Z. Jie, J. Liu, M. Shu, Y. Ying and H. Yang, *Talanta*, 2022, **236**, 122892.

7 J. Wu, C. Li, Q. Chen and J. Zhao, *Dyes Pigm.*, 2021, **195**, 109709.
8 V. P. Reddy, E. Sinn and N. Hosmane, *J. Organomet. Chem.*, 2015, **798**, 5–12.
9 P. Molina, F. Zapata and A. Caballero, *Rev*, 2017, **117**, 9907.
10 D. T. Thompson, *Gold Bull.*, 2001, **34**, 133.
11 K. Matsubara, A. Akane, C. Maseda and H. Shiono, *Forensic Sci. Int.*, 1990, **46**, 203–208.
12 S. Chakraborty, S. Paul, P. Roy and S. Rayalu, *Inorg. Chem. Commun.*, 2021, **128**, 108562.
13 D. Udhayakumari, *Sens. Actuators, B*, 2018, **259**, 1022–1057.
14 H. Wan, Q. Xu, P. Gu, H. Li, D. Chen, N. Li, J. He and J. Lu, *J. Hazard. Mater.*, 2021, **403**, 123656.
15 D. Shan, C. Mousty and S. Cosnier, *Anal. Chem.*, 2004, **76**, 178–183.
16 G. Balamurugan, P. Venkatesan, S. P. Wu and S. Velmathi, *RSC Adv.*, 2016, **6**, 24229–24235.
17 P. J. R. de Rivera, M. R. de Rivera, F. Socorro and M. R. de Rivera, *Measurement*, 2021, **186**, 110134.
18 H. Tavallali, G. Deilamy-Rad, A. Parhami, R. Zebarjadi, A. Najafi-Nejad and N. Mosallanejad, *Anal. Biochem.*, 2022, **637**, 114475.
19 H. Battula, S. Muduli, S. P. Bandi, S. Kapoor, S. Mishra, H. Aggarwal, V. V. krishna Venuganti and S. Jayanty, *J. Photochem. Photobiol., A*, 2022, **426**, 113748.
20 T. S. Aysha, M. B. I. Mohamed, M. S. El-Sedik and Y. A. Youssef, *Dyes Pigm.*, 2021, **196**, 109795.
21 S. Sawminathan, S. Munusamy, S. Manickam, D. Jothi and S. KulathuIyer, *Dyes Pigm.*, 2021, **196**, 109755.
22 D. Jothi and S. K. Iyer, *J. Photochem. Photobiol., A*, 2022, 113802.
23 D. Jothi, S. Munusamy and S. K. Iyer, *J. Photochem. Photobiol., A*, 2021, **420**, 113491.
24 S. Munusamy, V. P. Muralidharan and S. K. Iyer, *Sens. Actuators, B*, 2017, **250**, 244–249.
25 R. Chandra, A. Ghorai and G. K. Patra, *Sens. Actuators, B*, 2018, **255**, 701–711.
26 H. S. Jung, J. H. Han, Z. H. Kim, C. Kang and J. S. Kim, *Org. Lett.*, 2011, **13**, 5056–5059.
27 M. T. Gabr and F. C. Pigge, *Dalton Trans.*, 2018, **47**, 2079–2085.
28 P. Anzenbacher, D. S. Tyson, K. Jursíková and F. N. Castellano, *J. Am. Chem. Soc.*, 2002, **124**, 6232–6233.
29 S. Kim, J. Y. Noh, S. J. Park, Y. J. Na, I. H. Hwang, J. Min, C. Kim and J. Kim, *RSC Adv.*, 2014, **4**, 18094–18099.
30 C. Zhang, C. Liu, B. Li, J. Chen, H. Zhang, Z. Hu and F. Yi, *New J. Chem.*, 2015, **39**, 1968–1973.
31 P. M. Reddy, S.-R. Hsieh, C.-J. Chang and J.-Y. Kang, *J. Hazard. Mater.*, 2017, **334**, 93–103.
32 Q. Niu, T. Sun, T. Li, Z. Guo and H. Pang, *Sens. Actuators, B*, 2018, **266**, 730–743.
33 A. Mouradzadegun and F. Abadast, *Chem. Commun.*, 2014, **50**, 15983–15986.
34 P. Jayasudha, R. Manivannan and K. P. Elango, *Sens. Actuators, B*, 2015, **221**, 1441–1448.
35 N. Niamnont, A. Khumsri, A. Promchat, G. Tumcharern and M. Sukwattanasinitt, *J. Hazard. Mater.*, 2014, **280**, 458–463.
36 D. Jothi, S. Munusamy, S. Enbanathan and S. K. Iyer, *RSC Adv.*, 2022, **12**, 8570–8577.
37 P. G. Rao, B. Saritha and T. S. Rao, *J. Photochem. Photobiol., A*, 2019, **372**, 177–185.
38 S. Erdemir and S. Malkondu, *Talanta*, 2021, **231**, 122385.
39 R. Shanmugapriya, P. S. Kumar, S. Ponkarpagam, C. Nandhini, K. Vennila, A. G. Al-Sehemi, M. Pannipara and K. P. Elango, *J. Mol. Struct.*, 2022, **1251**, 132081.
40 J. Li, Z. Chang, X. Pan, W. Dong and A.-Q. Jia, *Dyes Pigm.*, 2019, **168**, 175–179.
41 N. Mergu, J. H. Moon, H. Kim, G. Heo and Y.-A. Son, *Sens. Actuators, B*, 2018, **273**, 143–152.
42 F. Huo, J. Kang, C. Yin, J. Chao and Y. Zhang, *Sens. Actuators, B*, 2015, **215**, 93–98.
43 J. Li, W. Wei, X. Qi, G. Zuo, J. Fang and W. Dong, *Sens. Actuators, B*, 2016, **228**, 330–334.
44 D. Jothi, S. Munusamy, S. Enbanathan and S. K. Iyer, *RSC Adv.*, 2022, **12**, 8570–8577.
45 S. Enbanathan, S. Manickam, S. Munusamy, D. Jothi, S. M. Kumar and S. K. Iyer, *New J. Chem.*, 2022, **46**(14), 6570–6576.
46 D. Jothi, S. Munusamy, S. Enbanathan and S. K. Iyer, *J. Photochem. Photobiol., A*, 2022, 114269.